Kinematics Analysis and Singularity Avoidance of a Parallel Mechanism with kinematic redundancy

chaoyu shen
China Waterborne Transport Research Institute https://orcid.org/0000-0002-4694-8548
Haibo Qu (hbqu@bjtu.edu.cn)
China Waterborne Transport Research Institute https://orcid.org/0000-0003-3053-7901
Sheng Guo
Beijing Jiaotong University
Xiao Li
Beijing Jiaotong University

Original Article

Keywords: Parallel mechanism, Kinematic redundancy, Singularity, Simulation analysis

Posted Date: October 28th, 2021

DOI: https://doi.org/10.21203/rs.3.rs-1016542/v1

Kinematics Analysis and Singularity Avoidance of a Parallel Mechanism with kinematic redundancy

Chaoyu Shen[1,2], Haibo Qu[1*], Sheng Guo[1] and Xiao Li[1]

Correspondence to: Haibo Qu / hbqu@bjtu.edu.cn

Abstract The kinematic redundancy is considered as a way to improve the performance of parallel mechanism. In this paper, the kinematics performance of a three degree-of-freedom parallel mechanism with kinematic redundancy (3-DOF PM-KR) and the influence of redundant part on the PM-KR are analyzed. Firstly, the kinematics model of the PM-KR is established. The inverse solutions, the Jacobian matrix and the workspace of the PM-KR are solved. Secondly, the influence of the redundant redundancy on the PM-KR has been analyzed. Since there exists kinematic redundancy, the PM-KR possesses the fault-tolerant performance. By locking one actuated joint or two actuated joints simultaneously, the fault-tolerant workspace are obtained. When the position of the redundant part is changed, the workspace and singularity will be changed. The results show that the kinematic redundancy can be used to avoid the singularity. Finally, the simulations are performed to prove the theoretical analysis.

Keywords: Parallel mechanism; Kinematic redundancy; Singularity; Simulation analysis

1 Introduction

The Parallel mechanism is defined as a closed-loop kinematic chain mechanism whose end-effector is linked to the fixed base by several independent kinematic chains [1]. Many scholars claim that it has some advantages of high stiffness, high accuracy, and small error accumulation. However, it also has some disadvantages, such as many singularities in the workspace and difficulty to eliminate self-motion. Many scholars tried to improve the performance of the parallel mechanism by adding redundant actuators or redundant structures.

Scientist Merlet [2] pointed out that redundancy is a way to improve parallel mechanism's performance. For parallel mechanisms with redundant actuators, the number of actuators is greater than the mobility of the parallel mechanism. Many researchers proved that redundant actuators could be used to solve the forward kinematics [3], avoid singularities [4,5], and optimize the distribution of force/torque [6,7,8]. However, the redundant actuators need strict movement coordination, which increases the control difficulty.

In order to overcome the shortcomings and realize the self-coordination between inputs and outputs, some scholars proposed to design parallel mechanisms with redundant kinematic structure. For parallel mechanism with kinematic redundancy, the mobility of the parallel mechanism is equal to the number of actuators but greater than the degree of freedom of the moving platform. Except the earlier studies [9,10,11], many researchers play great attentions on parallel mechanism with kinematic redundancy in recent years.

The Gosselin group conducted a lot of relevant analysis for the kinematically redundant parallel mechanism. Wen and Gosselin [12,13] proposed a (6+3) DOF kinematically redundant hybrid parallel robot and did a lot of kinematic analysis on it, and proved all the singularities of this mechanism are avoidable, indicating that this mechanism has a large workspace. They introduced a new method for detecting mechanical interferences between two links that are not directly connected, proposed for evaluating the workspace of the kinematically redundant parallel mechanism. Landuré and Gosselin [14] proposed a spherical parallel robot and proved that its workspace is huge. The analysis of the mechanism's singularity shows that the kinematically redundant parallel mechanism's workspace has design advantages. Mats and Gosselin [15] provides an analysis of a class of kinematically redundant parallel manipulators. They explored the singularity of this kind of parallel mechanism with kinematic redundancy by using the screw theory.

Many researchers explored the type synthesis of the parallel mechanism with kinematic redundancy. Qu [16,17] discussed the difference between a parallel manipulator's mobility and the relative degree of freedom. Based on the proposed relative degree-of-freedom criterion, they performed the type synthesis of the parallel manipulator with open-loop limbs or closed-loop limbs. Besides, they synthesized a kind of kinematically redundant parallel manipulator based on the modified G-K formula and RDOF criterion. Li [18] summarized several types of parallel mechanisms with 2R1T redundant parallel mechanisms and 2T1R redundant parallel mechanisms, and the results showed that all kinematic redundant mechanisms have good performance. Wang [19] proposed a hybrid strategy based on the combination of linear decoupling geometric analysis method and high-order convergence iteration method to solve the positive solution of parallel mechanism. Wang [20] analyzed the topology and kinematics of the 6-DOF parallel mechanism with kinematic redundancy, and then solved the direct solution of the mechanism.

Studies had shown that the kinematics redundant parallel mechanism has dramatically improved its kinematic performance in its mechanism singularity and workspace [21,22,23]. Li [24] proposed a new 3-PRPR parallel mechanism with kinematic redundancy, and analyzed the workspace of the mechanism under different trace, and proved that the workspace of the parallel mechanism with kinematic redundancy was significantly increased. Zhao [25] proposed a 3-

RPS/3-SPS parallel mechanism with redundant limbs and defined the evaluation index of the workspace. The results showed that the workspace and kinematics performance of the mechanism was improved. Jin [26] designed a type of 2RIT kinematics redundant parallel mechanism, analyzed the inverse kinematics and workspace of this mechanism, and proved that it had a larger two-dimensional rotation angle of the workspace. By studying the singularity and workspace of the parallel mechanism with kinematic redundancy, changing the mechanism's structure can be used to optimize the geometry of the mechanism.

For the redundant kinematics parallel mechanism, the influence of redundant kinematics components on the mechanism is explored by solving the statics and dynamics. Qu [28] analyzed the statics of a planar parallel mechanism with kinematic redundancy, and its actuated torque was significantly lower than that of the 3-RRR parallel mechanism. This showed that the introduction of the kinematic redundant components could change the force transmission of the mechanism and improve the statics performance. Rahmat Abadi [29] took a 3-RPRR planar kinematics redundant mechanism as the research object and used the principle of virtual work to obtain the inverse dynamics of the mechanism. The comparison with the non-redundant mechanism showed that the mechanism could avoid the singular position by adding redundant components. Schreiber [30] studied the dynamic trace planning for a 3-DOF space parallel robot and established its dynamic model.

The above analysis proved that adding kinematic redundant components to the parallel mechanism has a positive effect on the optimization of mechanical structure and the improvement of mechanical performance. This paper takes a 3-DOF parallel mechanism with kinematic redundancy (PM-KR) as the research object. By building its structure model, the singular position and workspace of the mechanism can be solved. Through analyzing the kinematic redundant component's effect on the singularity and workspace , we know that the parallel mechanism with kinematic redundancy has different kinematic performance compared to the general parallel mechanism. The kinematics simulation of the three singular positions of the mechanism is carried out, exploring the impact of changes in the structural parameters of redundant components on the performance of avoiding singular positions, which can prove that this kinematic redundant structure design of the mechanism has obvious advantages.

2 Kinematics Analysis of PM-KR

2.1 Structure description

The studied parallel mechanism with kinematic redundancy is shown in Fig. 1. This parallel mechanism consists of a fixed base, an equilateral triangular moving platform, three kinematic limbs with the same structure and a lifting platform. Qu[17] proved that the moving platform has three independent movements, and the mobility of the whole mechanism is equal to 4. The 4 prismatic joints connected to the base are selected as the actuated joints, respectively actuated joints L_1, L_2, L_3 and L_4.

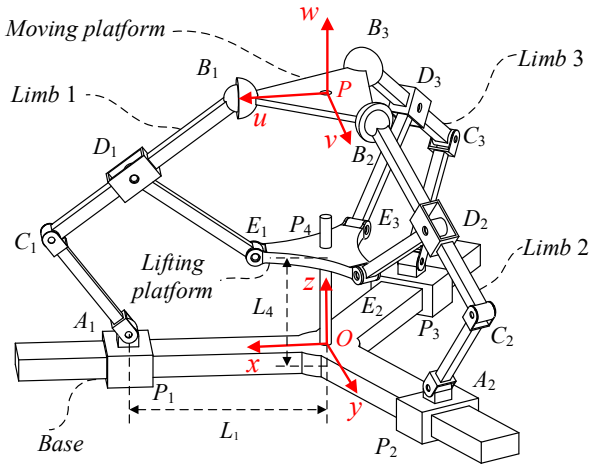

Figure 1 Three-dimensional structure model.

One side of the limbs of the mechanism is connected to the base by a prismatic joint, and these three prismatic joints are all actuated joints. The other side is connected to the moving platform through a ball joint. The rotation joints of each limb are passive and are parallel to each other. Ai , Ci , Di and Ei are the center points of the rotating joints in each limb, Bi is the center point of the spherical joint in each limb, P_4 is the center point of the lifting platform, the link $CiBi$ and the link $DiEi$ pass through the rotating joint Di Connect, Di is a point of the link $CiBi$. Establish the coordinate systems O-xyz and P-uvw with the x-axis and the u-axis perpendicular to the axes of revolute joints of the limb 1.

2.2 Kinematics inverse solution

The specific process to solve the inverse kinematics solution of the mechanism is shown in Fig. 2.

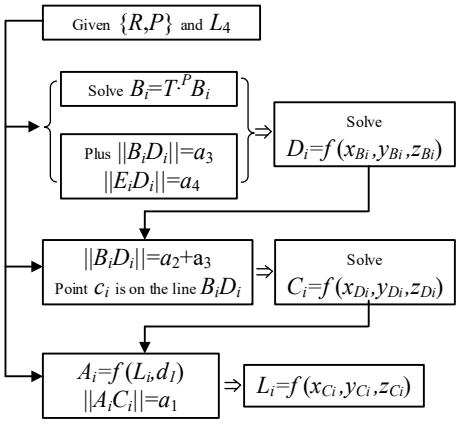

Figure 2 The inverse kinematics solution process of the mechanism.

As shown in Fig. 3, it is the geometric structure of the mechanism. The base coordinate system $\{O\}$ is O-xyz with the y-axis pointing out of the paper and x-axis aligned with the axis of prismatic joint P_i. The moving platform coordinate system $\{P\}$ is P-uvw with w-axis perpendicular to the u-axis and the v-axis.

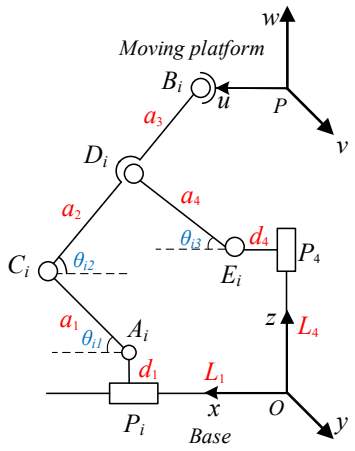

Figure 3 The geometric structure of the mechanism.

The position of the center point P of the moving platform can be defined as shown in the following Eq. (1).

$$\overrightarrow{{}^{O}P}=\begin{bmatrix}p_x & p_y & p_z\end{bmatrix}^{\mathrm{T}} \tag{1}$$

Besides, the rotation matrix ${}^{O}R_P$ is used to define the position of the moving platform relative to the base coordinate system $\{O\}$, using the expression of pitch-roll-yaw, as shown in the following Eqs. (2)-(3).

$${}^{O}R_P=\begin{bmatrix}u_x & v_x & w_x\\ u_y & v_y & w_y\\ u_z & v_z & w_z\end{bmatrix} \tag{2}$$

$${}^{O}R_P=R_z(\gamma)R_y(\beta)R_x(\alpha)=\begin{bmatrix}c\beta c\gamma & c\gamma s\alpha s\beta-c\alpha s\gamma & c\alpha c\gamma s\beta+s\alpha s\gamma\\ c\beta s\gamma & s\alpha s\beta s\gamma+c\alpha c\gamma & c\alpha s\beta s\gamma-c\gamma s\alpha\\ -s\beta & c\beta s\alpha & c\alpha c\beta\end{bmatrix} \tag{3}$$

In the above Eqs. (2)-(3), α, β and γ are respectively expressed as Euler angles of the moving platform about the x, y,and z axes. Therefore, according to the Eq. (4), the midpoint's representation on the moving platform in $\{O\}$ can be obtained.

$$\overrightarrow{{}^{O}P}={}^{O}R_P\,\overrightarrow{{}^{P}P}+\overrightarrow{OP} \tag{4}$$

The positions of the three spherical joints in the moving platform coordinate system $\{B\}$ are expressed as.

$$\begin{cases}\overrightarrow{{}^{P}B_1}=\begin{bmatrix}r & 0 & 0\end{bmatrix}^{\mathrm{T}}\\ \overrightarrow{{}^{P}B_2}=\begin{bmatrix}-r/2 & \sqrt{3}r/2 & 0\end{bmatrix}^{\mathrm{T}}\\ \overrightarrow{{}^{P}B_3}=\begin{bmatrix}-r/2 & -\sqrt{3}r/2 & 0\end{bmatrix}^{\mathrm{T}}\end{cases} \tag{5}$$

According to the Eq. (5), the transformation formula of the three spherical joints can be obtained, as shown in the following Eq. (6).

$$\overrightarrow{{}^{O}B_i}={}^{O}R_P\,\overrightarrow{{}^{P}B_i}+\overrightarrow{OP} \tag{6}$$

Through calculation, the basic coordinate vector representation of B_i (i=1,2,3) can be obtained, as shown in the following Eqs. (7)-(9).

$$\overrightarrow{{}^{O}B_1}=\begin{bmatrix}p_x+ru_x\\ p_y+ru_y\\ p_z+ru_z\end{bmatrix}=\begin{bmatrix}p_x+r\cos\beta\cos\gamma\\ p_y+r\cos\beta\sin\gamma\\ p_z-r\sin\beta\end{bmatrix} \tag{7}$$

$$\overrightarrow{{}^{O}B_2}=\begin{bmatrix}p_x-\frac{1}{2}r\left(\cos\beta\cos\gamma+\sqrt{3}(-\cos\gamma\sin\alpha\sin\beta+\cos\alpha\sin\gamma)\right)\\ p_y-\frac{1}{2}r\cos\beta\sin\gamma+\frac{\sqrt{3}}{2}r(\cos\alpha\cos\gamma+\sin\alpha\sin\beta\sin\gamma)\\ p_z+\frac{1}{2}r(\sqrt{3}\cos\beta\sin\alpha+\sin\beta)\end{bmatrix} \tag{8}$$

$$\overrightarrow{{}^{O}B_3}=\begin{bmatrix}p_x+\frac{1}{2}r\left(-\cos\beta\cos\gamma+\sqrt{3}(-\cos\gamma\sin\alpha\sin\beta+\cos\alpha\sin\gamma)\right)\\ p_y-\frac{1}{2}r\left(\sqrt{3}\cos\alpha\cos\gamma+(\cos\beta+\sqrt{3}\sin\alpha\sin\beta\sin\gamma)\right)\\ p_z+\frac{1}{2}r(-\sqrt{3}\cos\beta\sin\alpha+\sin\beta)\end{bmatrix} \tag{9}$$

The base coordinate vector representation of the point A_i(i=1,2,3) is shown in the following Eq. (10).

$$\begin{cases}\overrightarrow{{}^{O}A_1}=\begin{bmatrix}L_1 & 0 & d_1\end{bmatrix}^{\mathrm{T}}\\ \overrightarrow{{}^{O}A_2}=\begin{bmatrix}-1/2L_2 & \sqrt{3}/2L_2 & d_1\end{bmatrix}^{\mathrm{T}}\\ \overrightarrow{{}^{O}A_3}=\begin{bmatrix}-1/2L_3 & -\sqrt{3}/2L_3 & d_1\end{bmatrix}^{\mathrm{T}}\end{cases} \tag{10}$$

According to the position coordinates of $\boldsymbol{A_i}$ and $\boldsymbol{B_i}$, the distance between the joint A_i and the joint B_i can be calculated, as shown in the following Eq. (11).

$$\overrightarrow{A_iB_i}=\overrightarrow{B_i}-\overrightarrow{A_i} \tag{11}$$

Set the vector $\vec{s}_i$ in three directions on the base, as shown in the following Eq. (12).

$$\begin{cases}\overrightarrow{{}^{O}s_1}=\begin{bmatrix}0 & 1 & 0\end{bmatrix}^{\mathrm{T}}\\ \overrightarrow{{}^{O}s_2}=\begin{bmatrix}\sqrt{3} & 1 & 0\end{bmatrix}^{\mathrm{T}}\\ \overrightarrow{{}^{O}s_3}=\begin{bmatrix}-\sqrt{3} & 1 & 0\end{bmatrix}^{\mathrm{T}}\end{cases} \tag{12}$$

Because $\vec{s}_i$ is perpendicular to $\overrightarrow{A_iB_i}$, the dot product of the two vectors is equal to 0, and the expressions of p_x , p_y and γ can be obtained, as shown in the following Eqs. (13)-(15).

$$p_x = -\frac{r\left(\cos^2\alpha - \cos^2\beta + \sin^2\alpha\sin^2\beta\right)}{2\sqrt{\left(1+\cos\alpha\cos\beta\right)^2}} \tag{13}$$

$$p_y = -\frac{r\cos\beta\sin\alpha\sin\beta}{\sqrt{\left(1+\cos\alpha\cos\beta\right)^2}} \tag{14}$$

$$\gamma = \arctan\left[\frac{\cos\alpha+\cos\beta}{\sqrt{\left(1+\cos\alpha\cos\beta\right)^2}}, \frac{\sin\alpha\sin\beta}{\sqrt{\left(1+\cos\alpha\cos\beta\right)^2}}\right] \tag{15}$$

According to the above method, the coordinate representation of the remaining joints on the limb can be obtained sequentially.

The inverse solution of the mechanism is that the parameters α, β and z_p of the moving platform are known, and the actuated lengths L_1, L_2 and L_3 of the input prismatic joints are calculated. According to the vector closed-loop principle, a vector closed-loop equation is established in a limb of this mechanism, as shown in Fig. 4 below, the four vector combinations $\boldsymbol{OA_1}$, $\boldsymbol{A_1C_1}$, $\boldsymbol{C_1B_1}$, $\boldsymbol{B_1O}$ are selected as the closed-loop.

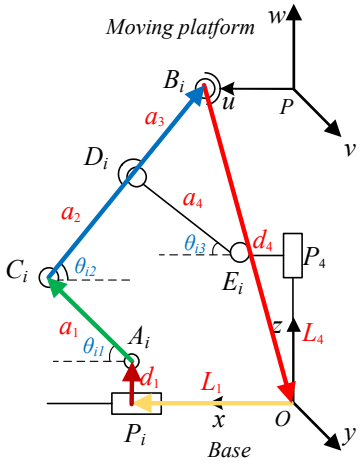

Figure 4 Diagram of closed-loop 1.

According to Fig. 4, the closed-loop equation 1 of limb 1 can be obtained, as shown in the following Eq. (16).

$$\overrightarrow{OP_1} + \overrightarrow{P_1A_1} + \overrightarrow{A_1C_1} + \overrightarrow{C_1B_1} = \overrightarrow{OB_1} \tag{16}$$

According to the above Eq. (16), and replaced with the structural parameters of the mechanism, as shown in the following Eq. (17).

$$\begin{bmatrix} x_{a1} \\ 0 \\ z_{a1} \end{bmatrix} + \begin{bmatrix} a_1\cos\theta_{11} \\ 0 \\ a_1\sin\theta_{11} \end{bmatrix} + \begin{bmatrix} -\left(a_2+a_3\right)\cos\theta_{12} \\ 0 \\ \left(a_2+a_3\right)\sin\theta_{12} \end{bmatrix} = \begin{bmatrix} x_{b1} \\ 0 \\ z_{b1} \end{bmatrix} \tag{17}$$

Because the mechanism is a parallel mechanism with kinematic redundancy, its redundant structure is a lifting platform. The two closed-loop equations of the limb are solved simultaneously, as shown in Fig. 5 and 6 below.

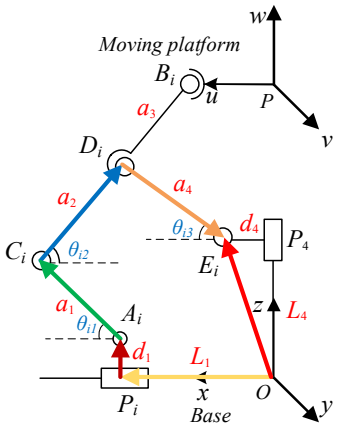

Figure 5 Diagram of closed-loop 2.

According to Fig. 5, the closed-loop equation 2 of limb 1 can be obtained as follows, as shown in the following Eq. (18).

$$\overrightarrow{OP_1} + \overrightarrow{P_1A_1} + \overrightarrow{A_1C_1} + \overrightarrow{C_1D_1} + \overrightarrow{D_1E_1} = \overrightarrow{OE_1} \tag{18}$$

According to the above Eq. (18), and replaced with the mechanism's structural parameters, as shown in the following Eq. (19).

$$\begin{bmatrix} x_{a1} \\ 0 \\ z_{a1} \end{bmatrix} + \begin{bmatrix} a_1\cos\theta_{11} \\ 0 \\ a_1\sin\theta_{11} \end{bmatrix} + \begin{bmatrix} -a_2\cos\theta_{12} \\ 0 \\ a_2\sin\theta_{12} \end{bmatrix} + \begin{bmatrix} -a_4\cos\theta_{13} \\ 0 \\ -a_4\sin\theta_{13} \end{bmatrix} = \begin{bmatrix} x_{e1} \\ 0 \\ z_{e1} \end{bmatrix} \tag{19}$$

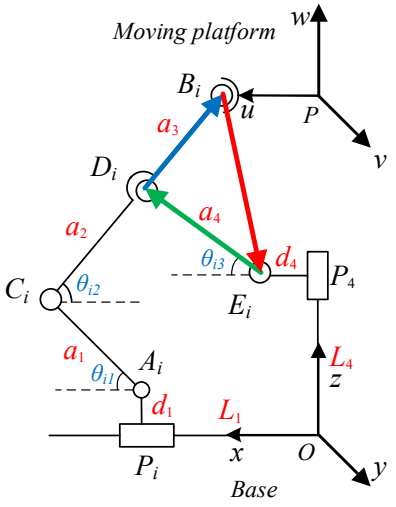

Figure 6 Diagram of closed-loop 3.

As shown in Fig. 6. The closed-loop equation 3 of limb 1 can be obtained, as shown in the following Eq. (20).

$$\overrightarrow{E_1D_1} + \overrightarrow{D_1B_1} = \overrightarrow{E_1B_1} \tag{20}$$

According to the above Eq. (20), and replaced with the structural parameters of the mechanism, as shown in the following Eq. (21).

$$\begin{bmatrix} a_4\cos\theta_{13} \\ 0 \\ a_4\sin\theta_{13} \end{bmatrix}+\begin{bmatrix} -a_3\cos\theta_{12} \\ 0 \\ a_3\sin\theta_{12} \end{bmatrix}=\begin{bmatrix} x_{b1}-x_{e1} \\ 0 \\ z_{b1}-z_{e1} \end{bmatrix} \tag{21}$$

Expand the above Eqs. (16)-(21) to get six equations, as shown in the following Eq. (22).

$$\begin{cases} x_{a1}+a_1\cos\theta_{11}-(a_2+a_3)\cos\theta_{12}=x_{b1} & \text{(a)} \\ z_{a1}+a_1\sin\theta_{11}+(a_2+a_3)\sin\theta_{12}=z_{b1} & \text{(b)} \\ x_{a1}+a_1\cos\theta_{11}-a_2\cos\theta_{12}-a_4\cos\theta_{13}=x_{e1} & \text{(c)} \\ z_{a1}+a_1\sin\theta_{11}+a_2\sin\theta_{12}-a_4\sin\theta_{13}=z_{e1} & \text{(d)} \\ a_4\cos\theta_{13}-a_3\cos\theta_{12}=x_{b1}-x_{e1} & \text{(e)} \\ a_4\sin\theta_{13}+a_3\sin\theta_{12}=z_{b1}-z_{e1} & \text{(f)} \end{cases} \tag{22}$$

According to the coordinate expressions of B_1 and E_1, take D_1 as the center of the circle, B_1D_1, and E_1D_1 as the radius. The equations of the two circles are listed respectively, and the coordinates of D_1 can be solved, as shown in the following Eqs. (23)-(24).

$$(x_{d1}-x_{b1})^2+(z_{d1}-z_{b1})^2=a_3{}^2 \tag{23}$$

$$(x_{d1}-x_{e1})^2+(z_{d1}-z_{e1})^2=a_4{}^2 \tag{24}$$

According to the coordinates of B_1 and D_1 and the tangent formula of the triangle, the size of θ_{13} can be solved, as shown in the following Eq. (25).

$$\theta_{13}=\arctan\frac{z_{d1}-z_{e1}}{x_{d1}-x_{e1}} \tag{25}$$

According to the closed-loop equation Eq. (22 e), the size of θ_{12} can be solved, as shown in the following Eq. (26).

$$\theta_{12}=\arccos\frac{-x_{b1}+x_{e1}+a_4\cos\theta_{13}}{a_3} \tag{26}$$

Simultaneously eliminating θ_{12} in the Eqs. (22 a) and (22 b), the following Eq. (27) can be obtained.

$$\begin{aligned} &a_1{}^2+(x_{a1}-x_{b1})^2+2a_1(x_{a1}-x_{b1})\cos\theta_{11}+ \\ &(z_{a1}-z_{b1})^2+2a_1(z_{a1}-z_{b1})\sin\theta_{11}=(a_2+a_3)^2 \end{aligned} \tag{27}$$

According to the above Eq. (27), the expression of θ_{11} can be obtained, as shown in the following Eq. (28).

$$\theta_{11}=\arctan\left(\begin{array}{l} \dfrac{-a_1(x_{a1}-x_{b1})\left(a_1{}^2-(a_2+a_3)^2+(x_{a1}-x_{b1})^2+(z_{a1}-z_{b1})^2\right)}{a_1{}^2\left((x_{a1}-x_{b1})^2+(z_{a1}-z_{b1})^2\right)}+ \\ \dfrac{\sqrt{-a_1{}^2\left(\left(-a_1+a_2+a_3\right)^2-(x_{a1}-x_{b1})^2-(z_{a1}-z_{b1})^2\right)}}{a_1{}^2\left((x_{a1}-x_{b1})^2+(z_{a1}-z_{b1})^2\right)} \\ \dfrac{\sqrt{\left((a_1+a_2+a_3)^2-(x_{a1}-x_{b1})^2-(z_{a1}-z_{b1})^2\right)(z_{a1}-z_{b1})^2}}{a_1{}^2\left((x_{a1}-x_{b1})^2+(z_{a1}-z_{b1})^2\right)} \end{array}\right) \tag{28}$$

According to Eq. (22 c), only the actuated parameter L_1 is unknown in the equation. By solving the equation, the expression equation of L_1 can be obtained, as shown in the following Eq. (29).

$$L_1=x_{e1}-a_1\cos\theta_{11}-a_2\cos\theta_{12}-a_4\cos\theta_{13} \tag{29}$$

In the same way, the expressions for actuated lengths L_2 and L_3 can be obtained by the closed-loop equations of limb 2 and limb 3, as shown in the following Eqs. (30)-(31).

$$L_2=-2x_{e2}-a_1\cos\theta_{21}+a_2\cos\theta_{22}+a_4\cos\theta_{23} \tag{30}$$

$$L_3=-2x_{e3}-a_1\cos\theta_{31}+a_2\cos\theta_{32}+a_4\cos\theta_{33} \tag{31}$$

2.3 Singularity analysis

The positive Jacobian matrix J_q is the relationship between the twist $\dot{\chi}$ of the motion platform expressed by the six-dimensional vector and the rate of changing $\boldsymbol{L}i$ of the actuated length, as shown in the following Eq. (32).

$$\dot{L}_i=J_q\dot{\chi} \tag{32}$$

The Jacobian matrix of the parallel mechanism with kinematic redundancy is the relationship between the angular velocity ω of the moving platform and the vector L_1, L_2, L_3 of the actuated joint change rate, as shown in the Eq. (33).

$$\dot{L}=\vec{J}\cdot\vec{\omega} \tag{33}$$

The relationship between the inverse Jacobian matrix J_x, the three-dimensional twist vector $\dot{\chi}$ of the moving platform, and the angular velocity ω is shown in the following Eq. (34).

$$\dot{\chi}=\begin{bmatrix} {}^A\vec{v}_p \\ \vec{\omega} \end{bmatrix}=J_x\omega \tag{34}$$

In the Eq. (34), $\dot{\chi}$ represents the moving platform's twist, ${}^A v_p$ is the speed of the moving platform, and ω is the angular velocity of the moving platform.

Select the closed-loop 2 of the limb1, 2, 3. According to the result of the inverse solution, the constraint equations of the limb 1, 2, and 3 are shown in the Eqs. (35)-(37).

$$\begin{aligned}&\left(x_{a1}-x_{e1}-a_2\times\cos\theta_{12}-a_4\cos\theta_{13}\right)^2+\\&\left(z_{a1}-z_{e1}+a_2\sin\theta_{12}-a_4\sin\theta_{13}\right)^2=a_1^{\ 2}\end{aligned}\tag{35}$$

$$\begin{aligned}&\left(2x_{a2}-2x_{e2}-a_2\cos\theta_{22}+a_4\cos\theta_{23}\right)^2+\\&\left(z_{a2}-z_{e2}+a_2\sin\theta_{22}-a_4\sin\theta_{23}\right)^2=a_1^{\ 2}\end{aligned}\tag{36}$$

$$\begin{aligned}&\left(2x_{a3}-2x_{e3}+a_2\cos\theta_{32}+a_4\cos\theta_{33}\right)^2+\\&\left(z_{a3}-z_{e3}+a_2\sin\theta_{32}-a_4\sin\theta_{33}\right)^2=a_1^{\ 2}\end{aligned}\tag{37}$$

Calculate the partial derivative of the time t in the actuated parameters L_1, L_2, L_3 and the moving platform motion parameters α, β, z_p. After simplification, the Eqs. (38)-(40) can be obtained.

$$e_1=e_{11}\times\dot{\alpha}+e_{12}\times\dot{\beta}+e_{13}\times\dot{z}_p+e_{14}\times\dot{L}_1\tag{38}$$

$$e_2=e_{21}\times\dot{\alpha}+e_{22}\times\dot{\beta}+e_{23}\times\dot{z}_p+e_{24}\times\dot{L}_2\tag{39}$$

$$e_3=e_{31}\times\dot{\alpha}+e_{32}\times\dot{\beta}+e_{33}\times\dot{z}_p+e_{34}\times\dot{L}_3\tag{40}$$

In Eqs. (38)~(40), e_{ij}(i=1,2,3 and j=1,2,3,4) respectively represent the result of the combination of the same type and the simplified expressions of the result in Eqs. (35)-(37). Because these expressions are too long, they are not shown in the paper.

Extracting the common parameter items in the above formula, the positive Jacobian matrix J_q and the inverse Jacobian matrix J_x can be obtained, as shown in the Eqs. (41)-(42).

$$J_q=\begin{bmatrix}e_{14}&0&0\\0&e_{24}&0\\0&0&e_{34}\end{bmatrix}\tag{41}$$

$$J_x=\begin{bmatrix}e_{11}&e_{12}&e_{13}\\e_{21}&e_{22}&e_{23}\\e_{31}&e_{32}&e_{33}\end{bmatrix}\tag{42}$$

Let $Det(J_x)$=0, take the actuated parameter L_4 as the structure parameter, and measure singularity diagram of the mechanism under L_4=80mm, as shown in Fig. 7 below.

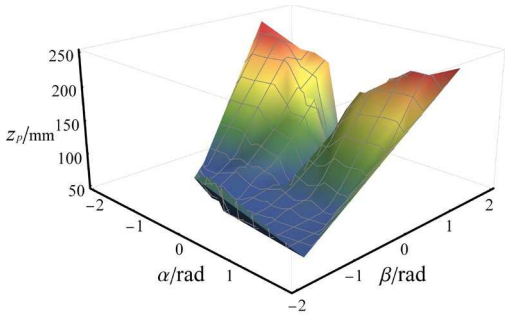

Figure 7 Singular diagram of mechanism when L_4=80mm.

Take z_p=150/170/190/210mm respectively, and measure the positive motion singular images of the mechanism under different z_p values, as shown in Fig. 8(a)~(d) below.

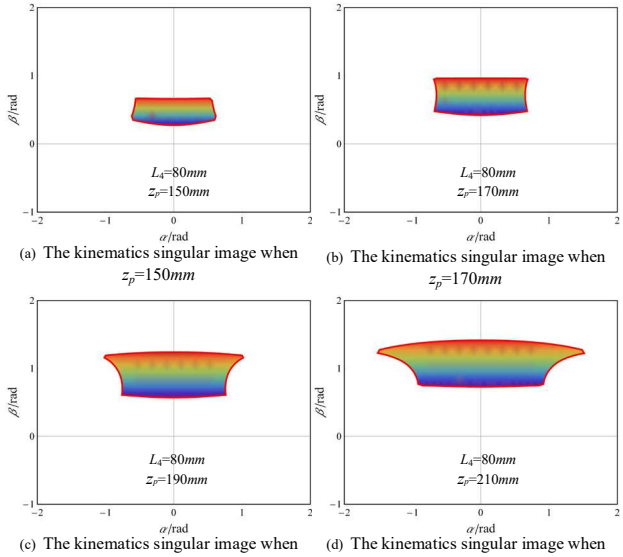

(a) The kinematics singular image when z_p=150mm (b) The kinematics singular image when z_p=170mm

(c) The kinematics singular image when z_p=190mm (d) The kinematics singular image when z_p=210mm

Figure 8 The singularity diagram of the mechanism when z_p takes different values (a)~(d).

By analyzing the Jacobian matrix and singular image of the mechanism, the singular position of the mechanism can be obtained[31,32,33]. When θ_{i1} =π/2 and θ_{i2}=0°of a limb, the mechanism will have a singular position①; When θ_{i1} =θ_{i2}=π/2 of the three limbs, the mechanism will have a singular position②; When θ_{i1} =0° of a limb, the mechanism produces a singular position③. The redundant components of the mechanism called lifting platform, its position will affect the singularity of the mechanism, which will be analyzed in the following content.

2.4 Workspace analysis

Set the structural parameters of the mechanism, d_1=30mm , a_1=114mm , a_2=92mm , a_3=115mm , d_4=62.68mm , r =78mm.

Analyze the workspace of the mechanism by adopting the workspace search method. Set the length of the actuating joint L_4 as a fixed value and obtain the point set where the workspace satisfies the

inverse solution of the mechanism. Finally, we can get the workspace diagram of the mechanism.

Analyzing limb 1, according to the expressions (25)-(28) of θ_{11}, θ_{12}, θ_{13} obtained by the inverse solution, substituting the above three equations into L_1 expression (29), we can get L_1's expression only have the moving platform kinematic parameters include α, β, and z_p. Similarly, we can get L_1, and L_2's expression only has the moving platform kinematic parameters include α, β, and z_p.

Set the value range of L_1, L_2, and L_3 to [50,200], the range of z_p to [50,350], and the value range of α and β to [-π/2, π/2]. L_4 is used as a structural parameter, and the workspace of the mechanism can be calculated when L_4=90*mm*, as shown in Fig. 9.

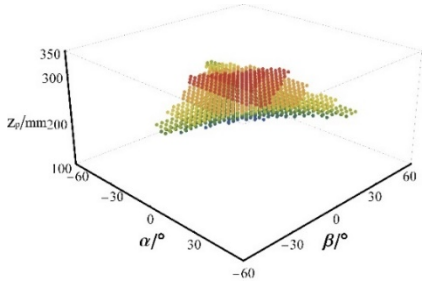

Figure 9 Three-dimensional point set diagram of the workspace.

Use the method of fitting a surface with a set of points and fitting the workspace point set of the mechanism, which can get the surface image of the workspace of the mechanism[34], as shown in Fig. 10 .

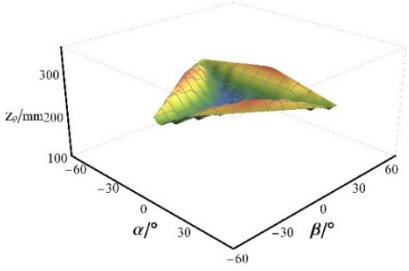

Figure 10 Three-dimensional curve diagram of workspace.

Analyze the workspace in the above Fig. 10, and solve the workspace diagram of the mechanism when z_p=230 /250 /270 /290*mm*.The moving platform parameters α and β are variables, and z_p is a fixed value. As shown in Fig. 11(a)~(d) below.

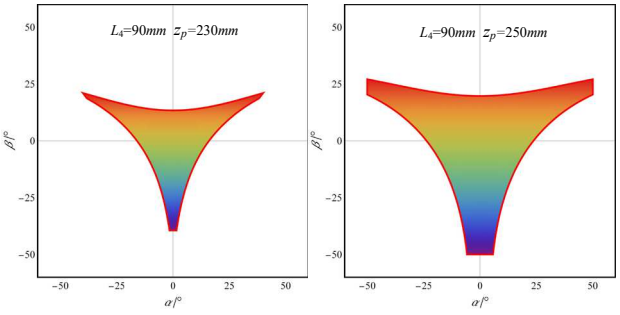

(a) Workspace diagram when z_p=230*mm* (b) Workspace diagram when z_p=250*mm*

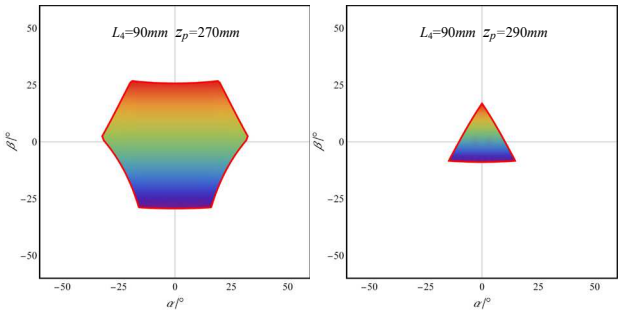

(c) Workspace diagram when z_p=270*mm* (d) Workspace diagram when z_p=290*mm*

Figure 11 Workspace diagram(a)~(d) of mechanism with different z_p values of L_4=90*mm*.

By analyzing the workspace images of the mechanism, we can get the changes of the moving platform kinematics parameters α and β when the moving platform parameter z_p is a fixed value. As shown in Table 1 below.

Table 1 Changes of kinematic parameters α and β of the moving platform.

z_p/mm	α/degree	β/degree
210	[-40,40]	[-42,24]
230	[-46,46]	[-48,28]
250	[-66,66]	[-66,34]
270	[-52,52]	[-50,34]
290	[-40,40]	[-32,36]
310	[-28,28]	[-16,32]

The above Table 1 shows that when the moving platform is in working condition, the maximum angle α and β of its rotation around the x and y axes can reach 66°. It shows that the moving platform of this mechanism has the characteristics of a large turning angle compared with the general parallel mechanism, which can meet the needs of specific working conditions.

3 The influence of redundant components on mechanism's kinematics

Adding a redundant part to a general parallel mechanism, the change of its structural parameters will affect the mechanism's kinematic characteristics, such as fault tolerance, workspace, and singularity[35]. This section conducts research on the impact of redundant components, analyzing the influence of the change of redundant part's parameters on the mechanism's kinematics.

3.1 Analysis of mechanism fault tolerance

Fault tolerance refers to the change in the mechanism's kinematic performance when a part of the mechanism fails. The better the fault-tolerant mechanism is, the smaller the difference in the mechanism's kinematics when the components fail. While for the mechanism with poor fault-tolerant performance, the components' failure will significantly impact the overall kinematics of the mechanism.

There are many indexes for measuring the fault tolerance performance of a mechanism, such as changes in the workspace, changes in actuated torque, and each joint's integrity. In measuring the fault-tolerant performance of the 3-DOF PM-KR, the change of the workspace is selected as the performance index. When a specific actuated joint of the mechanism fails, the influence on the mechanism's workspace will be very obvious. By observing the failure of one actuated joint of the mechanism and the failure of two actuated joints simultaneously, the change of the workspace of the mechanism is used to test the fault tolerance performance of the mechanism.

As shown in Fig. 12(a)~(f) below. It is the image of the workspace of the mechanism when the machine is operating normally, the actuated joint P_1 fails, the actuated joint P_1 and P_2 all fails. In the image, the moving platform kinematic parameters z_p=210/230/250/270/290/310*mm*, the height of the lifting platform L_4=90*mm*, the kinematics parameters of the moving platform $\alpha, \beta \in [-90°,90°]$, the actuated parameters $L_1, L_2, L_3 \in [50mm,200mm]$.

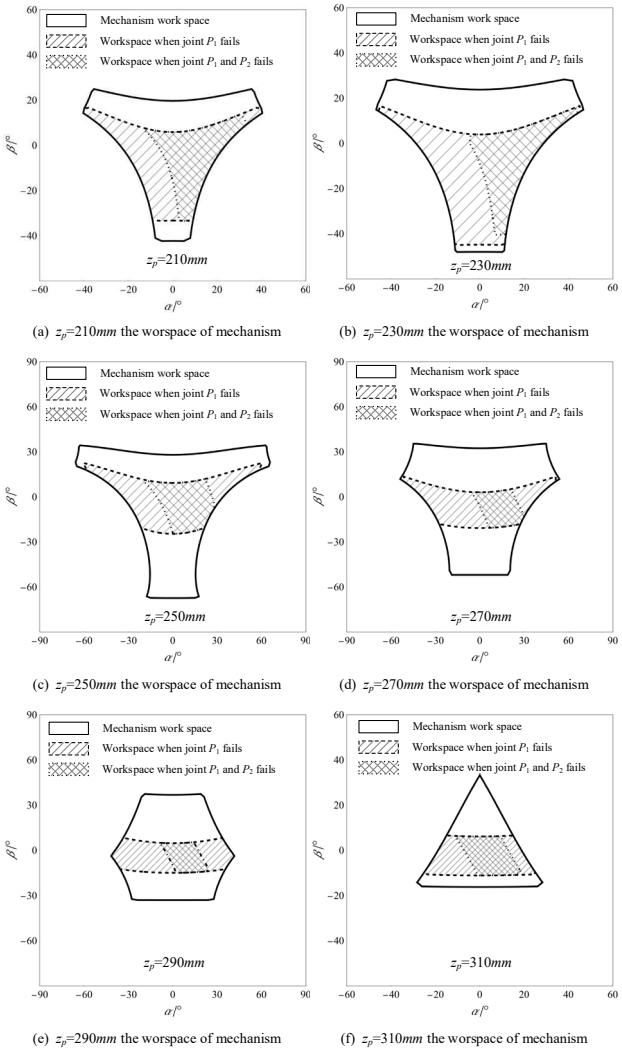

(a) z_p=210*mm* the worspace of mechanism (b) z_p=230*mm* the worspace of mechanism

(c) z_p=250*mm* the worspace of mechanism (d) z_p=270*mm* the worspace of mechanism

(e) z_p=290*mm* the worspace of mechanism (f) z_p=310*mm* the worspace of mechanism

Figure 12 Images (a)~(f) of the workspace when the L_4=90*mm*.

In order to analyze the fault-tolerant performance of the mechanism more deeply, the point search method is adopted, and the distance between the points is 3mm. First, the number of points in the workspace when the mechanism is normal is used as the base. Then the effective proportion of the workspace is analyzed when one actuated joint fails and two actuated joints fail simultaneously.

Table 2 Changes in the workspace of the mechanism.

z_p /*mm*	All points in the workspace	Number of workspace points when P_1 fails	Number of workspace points when P_1 and P_2 fail simultaneously
210	102	62 (60.78%)	33 (32.35%)
230	144	81 (56.25%)	34 (23.61%)
250	239	96 (60.78%)	42 (32.35%)
270	237	73 (30.80%)	23 (9.70%)
290	174	59 (33.90%)	16 (9.19%)
310	60	34 (56.67%)	16 (26.67%)

As shown in Table 2, it can be found that when the kinematic parameters of the moving platform z_p=210/230/250/310*mm*, the workspace when the actuated joint P_1 fails is about 60% of the normal workspace. When the actuated joint P_1 and P_2 fail simultaneously, the workspace is about equal to 30% of the normal workspace, indicating that the mechanism has better performance in this moving platform height.

When the moving platform's kinematic parameters are z_p=270/290*mm*, the workspace when the actuated joint P_1 fails is about 30% of the normal workspace. When the actuated joint P_1 and P_2 fail simultaneously, the workspace is about equal to 10% of the normal workspace. Compared with the fault tolerance of the mechanism obtained by the previous parameters, the mechanism's fault tolerance performance decreases.

The position where the actuated joint fails also has an impact on the fault tolerance of the mechanism. Measure the influence of the position where the actuated joint fails on the workspace. When the actuated joint P_1 fails, P_1 and P_2 fail simultaneously. As shown in Table 3, it is the influence of the drive joint failure's position on the workspace.

Table 3 The influence of the failure position of the actuated joint on the workspace.

The position where the actuated joint fails /*mm*	All points in the worksp ace	Number of workspace points when P_1 fails	Number of workspace points when P_1 and P_2 fail simultaneously
$L \in [50,100]$	4259	465(10.91%)	85(1.9%)
$L \in [100,150]$	4259	1264(29.68%)	505(11.86%)
$L \in [150,200]$	4259	2530(59.40%)	1819(42.71%)

Through the analysis of the above table 3, we can find that when the actuated joint fails at [50*mm*, 100*mm*], the workspace when the actuated joint P_1 fails is 10.91% of the normal workspace, the workspace when the actuated joint P_1 and P_2 fails simultaneously is 1.9% of the normal workspace. Because this position of the actuated joint is very close to the center of the whole mechanism, indicating that the actuated joint has a fault at this position, the fault tolerance of the mechanism is very poor. When the fault position of the actuated joint is [100*mm*, 150*mm*], the fault tolerance of the mechanism is improved, the workspace when the actuated joint P_1 fails is 29.68% of the normal workspace, the workspace when the actuated joint P_1 and P_2 fail simultaneously is 11.86% of the normal workspace. When the actuated joint's fault position is [150*mm*, 200*mm*], the fault tolerance of the mechanism is excellent, and the position of the actuated joint is the farthest from the center of the mechanism.

In summary, the 3-DOF PM-KR has a better fault tolerance. By analyzing the different height values z_p of the moving platform, the fault tolerance of the mechanism is improved, the workspace when the actuated joint P_1 fails is a maximum 60.78% of the normal workspace, the workspace when the actuated joint P_1 and P_2 fail simultaneously is maximum 32.35% of the normal workspace. At the same time, the position where the actuated joint fails also affects the fault tolerance of the mechanism. When the actuated joint fails is farther away from the center, the better the fault tolerance of the mechanism; on the contrary, the worse the fault tolerance of the mechanism.

3.2 The impact of redundant components on the workspace

Adding redundant components to the parallel mechanism will have a specific impact on the entire mechanism's workspace[36]. In the 3-DOF PM-KR, the lifting platform is connected with the link C_iB_i through three redundant link D_iE_i (i=1, 2, 3) in rotating joints. The lifting platform's height change will cause the position and posture of each link in the limb to change, which will affect the workspace of the mechanism.

Set the kinematic parameter z_p=250*mm* of the moving platform as a fixed value, and research the influence of the change of the height of the lifting platform L_4 on the kinematic parameters α and β of the moving platform. As shown in Fig. 13 below, it is the changing image of the workspace of the mechanism when L_4=60, 65, 70, 75*mm*.

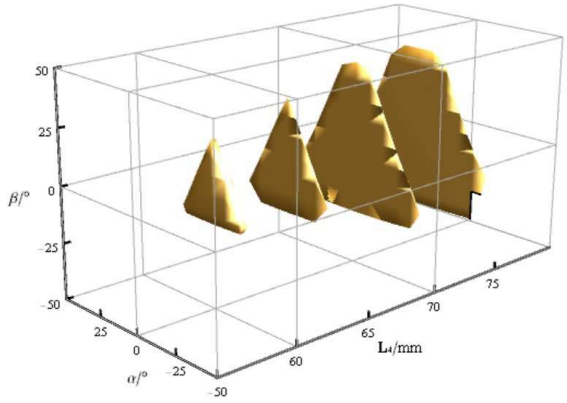

Figure 13 L_4=60~75*mm* workspace images of the mechanism.

By observing the workspace' image, we can conclude: With the increase of the value of L_4, the workspace of the mechanism also becomes larger, indicating that the increase in the structural parameters of redundant components will increase the workspace of the mechanism in this posture.

As shown in Fig. 14 below, it is an image of the workspace when L_4=80, 85, 90, 95*mm*. In this posture, when the value of L_4 increases from 80*mm* to 90*mm*, it can be observed that the workspace continues to increase; but when the value of L_4 continues to increase, because the lifting platform is located in the center of the entire mechanism, it's position has little influence on the posture of the limb, so the change of the workspace of the mechanism is not apparent.

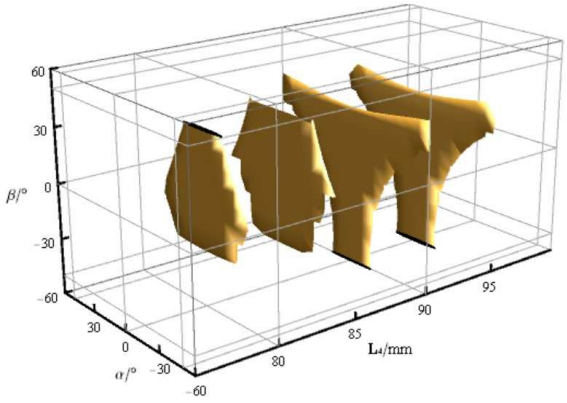

Figure 14 L_4=80~95*mm* workspace images of the mechanism.

Continue to increase the value of L_4, and take the changing image of the workspace when L_4=100, 105, 110, 115*mm*, as shown in Fig. 15 below. By observing the posture change of the workspace, we can explain that as the value of L_4 increases in this range, the mechanism's workspace is continuously reduced. Since the kinematic parameter z_p of the moving platform is set to a fixed value, in this posture, the lifting platform's height is constantly rising close to the moving platform. At this time, the mechanism's posture inhibits the movement of the limb, which makes the workspace of the mechanism continuously reduced.

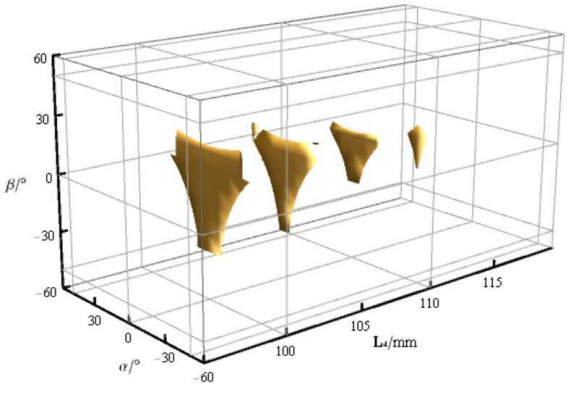

Figure 15 L_4=100~115*mm* workspace images of the mechanism.

Analyzing the mechanism's workspace shows that the change of the kinematic redundant part's position significantly impacts the workspace. When the lifting platform is at the starting position, as its

height value increases, the mechanism's workspace also becomes larger. Because each mechanism's workspace is fixed, when the position of the lifting platform reaches a specific height value, the change of the workspace of the mechanism is not obvious at this time. As the lifting platform's height value continues to increase, its position slowly approaches the moving platform of the mechanism, and the redundant part has a significant inhibitory effect on the movement of the limb, which causes the working space to occur significantly reduced.

3.3 The effect of redundant components on singularity

The structural parameter's change of the redundant part will impact the mechanism's kinematics, the most significant of which is to change the mechanism to avoid the singularity. Kinematics analysis obtains the Jacobian matrix of the mechanism and then solves the mechanism's singularity. Finally, we can obtain the singular position of the motion posture of the mechanism. Research on the kinematics parameter z_p value of the moving platform at different height values by changing the values of the redundant part L_4, the change of the singular images of the mechanism, and analyze the influence of the redundant components on the singularity avoidance of the mechanism.

As shown in Fig. 16 below, it is a singular image when the moving platform's kinematics parameter is z_p=150*mm*. When the value of L_4 is increased from 60*mm* to 100*mm*, the singular position's image is significantly reduced. Indicating that at this position, as the lifting platform's height value increased, the point set of the singular position of the mechanism continued to shrink.

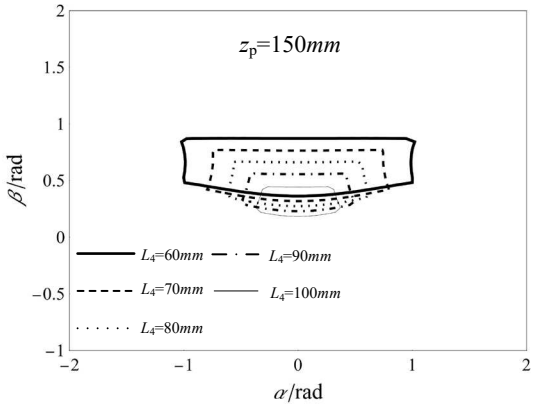

Figure 16 The image of the singular position of the mechanism when z_p=150*mm*.

When the value of actuated joint L_4 becomes larger, observe the change of the singular position's range of the mechanism. As shown in Fig. 17 below, it is a singular image when the kinematics parameter z_p of the moving platform of the mechanism is 170mm, the value range of L_4 is [60*mm*,100*mm*]. Compared with the singular images, when the height of the moving platform z_p is equal to 150*mm*, the point set of the mechanism's singular position at this height is increased. However, with the increase of the lifting platform's height, the point set of the mechanism's singular position has decreased significantly.

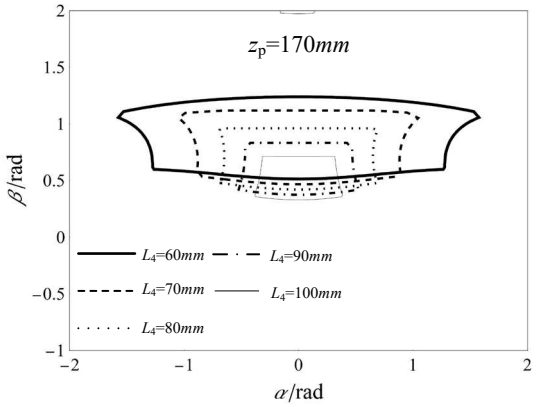

Figure 17 The image of the singular position of the mechanism when z_p=170*mm*.

Fig. 18 and Fig. 19 below show the singular image when the kinematic parameters of the moving platform z_p=190, 210*mm*, and the value range of L_4 is [60*mm*,100*mm*]. Research shows that when L_4 is a fixed value, as the value of the kinematic parameter z_p of the moving platform increases, the mechanism's singular position will continue to increase. Similarly, the change of the lifting platform's height value will affect the number of point sets of the singular positions.

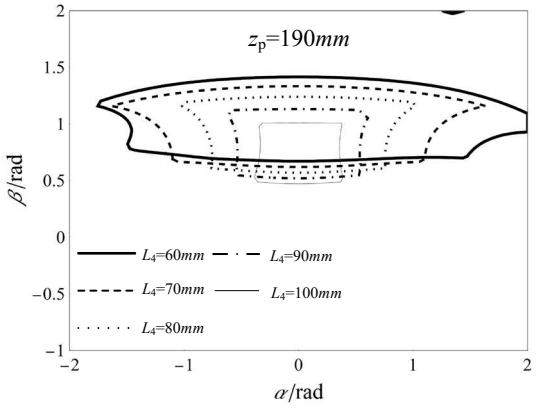

Figure 18 The image of the singular position of the mechanism when z_p=190*mm*.

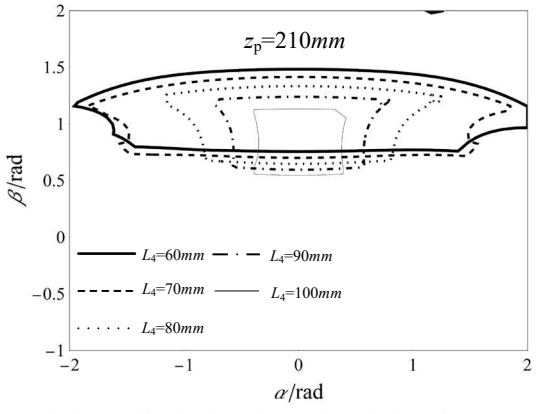

Figure 19 The image of the singular position of the mechanism when z_p=210*mm*.

Research shows that the change of the kinematic parameters of redundant components has an obvious influence on the mechanism's singular performance. When the moving platform is at a certain height,

the lifting platform's height change will reduce the singular position of the mechanism. It also shows that in this 3-DOF parallel mechanism, the addition of redundant components will positively affect the kinematics of the mechanism. When the mechanism is in a singular position, the mechanism's posture can be changed by changing the height of the lifting platform , which can achieve the purpose of avoiding singularity for the mechanism.

4 Simulation analysis

4.1 Simulations of mechanism avoiding singular position under three actions

In the previous section, the study found that the 3-DOF PM-KR has the characteristics of avoiding singularity. When the mechanism occurs singular positions, it can avoid the singular positions by changing the lifting platform's height. In this section, the Adams software is used to simulate the three singular positions of the mechanism. By changing the position of the lifting platform, the singular position of the mechanism can be avoided, which can verify the kinematic characteristics of the mechanism.

The mechanism's initial position is shown in Fig. 20. The height of the moving platform z_p=170*mm*, the deflection angle α=β=0°, the height of the lifting platform L_4=60*mm*, and the three actuated parameters on the base L_1=L_2=L_3=135*mm*. Set link A_iC_i as link 1, link D_iE_i as link 2, and link B_iC_i as link 3.

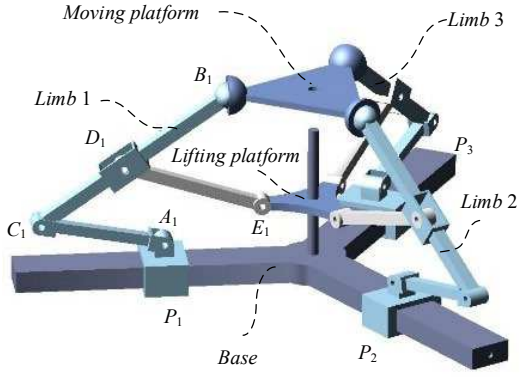

Figure 20 The initial position of the mechanism simulation.

As shown in Fig. 21(a), it is the first singular position of the mechanism, and the actuated joint's positions are L_1=215*mm*, L_2=L_3=100*mm*, L_4=60*mm*. At this time, the angle θ_{11} between the mechanism link 1 and the base is approximately equal to 90°, the link 1 of the limb 1 is approximately perpendicular to the base, and the link 3 is approximately parallel to the base, and the moving platform occurs a large angle. To avoid this singular position, it can increase the height of the lifting platform. When L_4 is equal to 100mm, the mechanism change's position and posture change, and the mechanism avoids the singular position, as shown in Fig. 21(b).

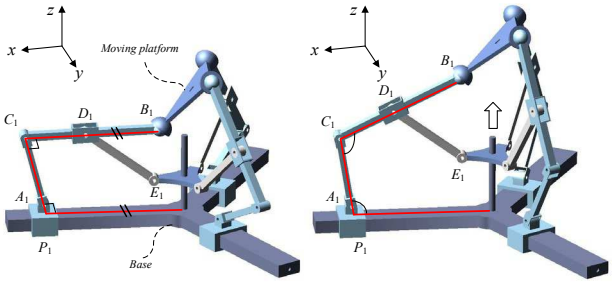

(a) Singular position 1 of mechanism (b) Avoiding singularity

Figure 21 Increasing the height of the lifting platform to avoid singularity at the singular position 1.

In the simulation, the first stage is the process of singular positions of the simulation mechanism, the simulation time is 0~5s; the second stage is the process of avoiding the singular positions of the mechanism, the simulation time is 5~8s. In the simulation using Adams software, the rotation angle of the moving platform, revolving joint and spherical joint are measured to judge whether the mechanism successfully completes the action of avoiding singular positions.

As shown in Fig. 22, it is the numerical change curve of the angle θ_{12} between link 1 and link 3 in the simulation of the mechanism. At the 5th second, indicate that link 1 and link 3 are approximately perpendicular at this time. When the position of the lifting platform increases, the angle between the two links changes, which indicate that the result of avoiding singular positions is obvious.

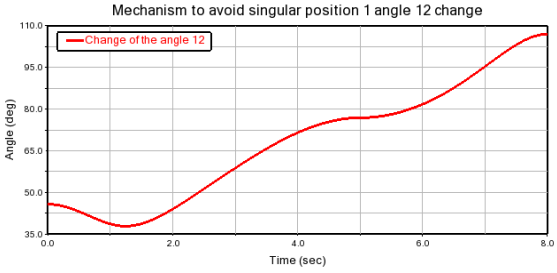

Figure 22 The change curve of angle θ_{12} when the mechanism avoids singular position 1.

Fig. 23 and Fig. 24 show the change curve of the angle of rotating joint C_1 and spherical joint B_1. At the 5th second, the deflection angle of the rotating joint C_1 is approximately 83.17°, which indicates that the joint has happened a very large rotation, and the position of the mechanism is gradually approaching the singular position. After the 5th second, as the lifting platform's height increased, the deflection angle of the joint gradually decreased. At the 8th second, the angle was 50.33°, and the angle of the spherical joint B_1 also changed, which indicates that the mechanism avoided singularity and returned to its normal position and posture.

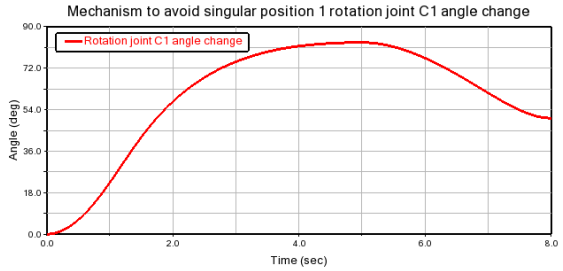

Figure 23 The change curve of the angle of the rotating joint C_1 when the mechanism avoids singular position 1.

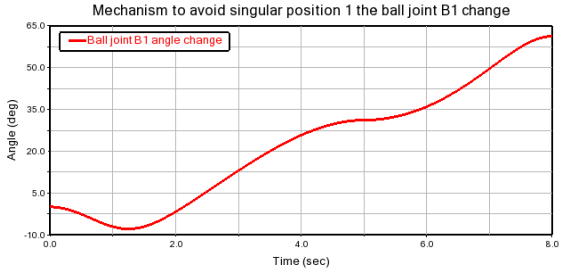

Figure 24 Angle change curve of spherical pair B_1 when the mechanism avoids singular position 1.

When the angle θ_{i1} and θ_{i2} of the mechanism are approximately equal to 90°, it is the mechanism's second singular position. The actuated joint's positions are L_1=L_2=L_3=100*mm* and L_4=100*mm*, the link 1 and link 3 of the three limbs are approximately perpendicular to the base, as shown in Fig. 25(a) below. By decreasing the height of the lifting platform, the mechanism can avoid singularity. When L_4=60mm, the posture of the limb changes and the height of the moving platform decreases simultaneously, and the mechanism returns to its normal posture, as shown in Fig. 25(b) below.

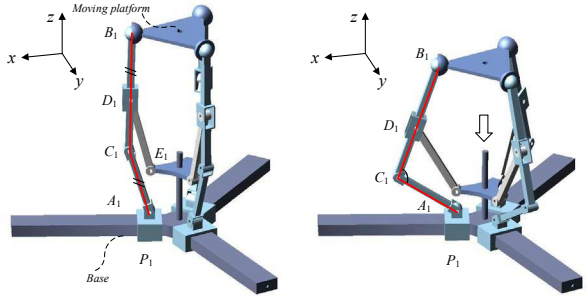

(a) Singular position 2 of mechanism (b) Avoiding singularity

Figure 25 Decreasing the height of the lifting platform to avoid singularity at the singular position 2.

As shown in Fig. 26 below, it is the change curve of the angle of rotating joint A_1 and rotating joint C_1 when the mechanism avoids singular position 2. In the 5th second, the rotating joint A_1 and rotating joint C_1 angles reached their maximum values of 68.34° and 126.45°. After the 5th second, the lifting platform's height is reduced, and the angles of the two rotating joints are reduced to 21.28° and 58.27°, which indicates that the mechanism has completed the avoidance of singular positions.

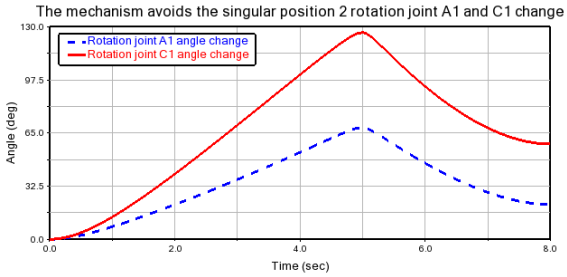

Figure 26 The change curve of the angle of the rotating joint A_1 and C_1 when the mechanism avoids singular position 2.

When the angle θ_{i1} approximately equal to 0° is the third singular position of the mechanism, the actuated joint's positions are L_1=L_2=L_3=143*mm* and L_4=60*mm*, and the link 1 of the three limbs is approximately parallel to the base, as follows, as shown in Fig. 27(a) below. By increasing the height of the lifting platform, the mechanism can avoid singularity. When L_4=100*mm*, the moving platform's height is increased, and the overall posture of the mechanism changes.

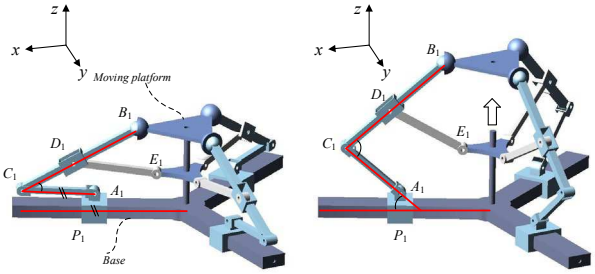

(a) Singular position 3 of mechanism (b) Avoiding singularity

Figure 27 Increasing the height of the lifting platform to avoid singularity at the singular position 3.

Fig. 28 and Fig. 29 below show the change curve of the angle of rotating joint A_1 and rotating joint D_1 when the mechanism avoids singular position 3. At the 5th second, the angle of the rotating joint A_1 is 4.18°, close to 0°, which indicates that link 1 is approximately parallel to the base at this position. If the actuated joint continues to move, the mechanism will be singular. After the 5th second, increasing the height of the lifting platform, the angle of the rotating joint A_1 has increased significantly to 43.21°, and the angle of the rotating joint D_1 has also changed significantly, which can indicate that the height of the lifting platform makes the mechanism successfully avoid the singularity.

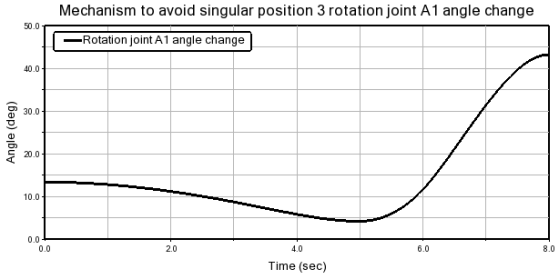

Figure 28 The change curve of the angle of the rotating joint A_1 when the mechanism

avoids singular position 3.

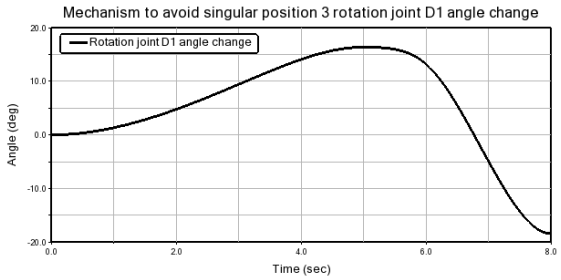

Figure 29 The change curve of the angle of the rotating joint D_1 when the mechanism avoids singular position 3.

4.2 Discussion

It is proved that the singularities can be avoided by changing the lifting platform's height when the mechanism is near or already in the singular positions. It also shows that the redundant kinematics part significantly improves the mechanism's kinematics performance and proves that the 3-DOF PM-KR has the advantages of structural design.

However, there are some problems in the simulation research. For example, the simulation of the mechanism is too ideal and doesn't fully consider the influence of the errors of the mechanism's materials and joints on the simulation results; When the mechanism reaches different singular positions, the force and deformation between joints and links will affect the overall mechanism. The parameters changing of the mechanism will also affect the effect of avoiding singular positions. In the follow-up research, we should solve these known problems as much as possible.

5 Conclusions

In this paper, the kinematics performance of a 3-DOF PM-KR and the influence of redundant part on the mechanism are analyzed. The main work and conclusions are drawn as follows:

(1) The kinematics of the PM-KR is solved. Since there are infinite number of solutions for the inverse kinematics of PM-KR, the actuated parameter of kinematic redundancy should be set as a constant firstly. Different actuated parameter of kinematic redundancy lead to different solutions.

(2) The kinematic redundancy affects the workspace and singularity of the PM-KR. The workspace and singularity can be adjusted by changing the parameters of redundant part. When the parameter of the redundant part is increased, the singularity of the mechanism can be significantly reduced, which achieves the purpose of avoiding singularities of 3-DOF PM-KR.

(3) Since the existed kinematic redundancy, the PM-KR possesses the fault-tolerant performance. When the position of the failed actuated joint is far away from the center, the fault-tolerant performance of the PM-KR is better.

Acknowledgments

This work supported by the Fundamental Research Funds for the Central Universities (2019JBM052) and the National Natural Science Foundation of China (51875033).

Authors' Contributions

CYS wrote the manuscript; HBQ was in charge of the whole trial, review and edition; SG and XL assisted with review. All authors read and approved the fnal manuscript.

Authors' Information

Chaoyu Shen, received his master's in Mechanical Engineering from Beijing Jiaotong University in 2021. Now he is an intern-researcher at China Waterborne Transport Research Institute, China.

Haibo Qu, is currently an Associate Professor in the School of Mechanical, Electronic and Control Engineering, Beijing Jiaotong University, China.

Sheng Guo, is currently a full professor, a vice director of Robotics Research Center, and a vice dean of School of Mechanical, Electronic and Control Engineering at Beijing Jiaotong University, China.

Xiao Li, is currently a PhD candidate in Mechanical Engineering at Beijing Jiaotong University, China.

Funding

Supported by the Fundamental Research Funds for the Central Universities (2019JBM052) and the National Natural Science Foundation of China (51875033).

Competing Interests

The authors declare no competing financial interests.

Author Details

[1] Robotics Research Center, School of Mechanical, Electronic and Control Engineering, Beijing Jiaotong University, Beijing 100044, China.[2] Port and Equipment Technology Research Center, China Waterborne Transport Research Institute, Beijing 100088, China.

References

[1] F. Wen, G. Yang, Overview of Parallel Robot Mechanisms [J]. *Mechanical Science and Technology*, 20 (1) (2001) 69-72.

[2] J-P Merlet, Redundant parallel manipulators[J]. *Laboratory Robotics and Automation*, 8(1) (2015) 17-24.

[3] G. F. Liu, Y. L. Wu, and X. Z. Wu, et al., Analysis and control of redundant parallel manipulators, Proceedings 2001 ICRA. *IEEE International Conference on Robotics and Automation*, (2001) 3748-3754.

[4] H. B. Liao, T. M. Li and X. Q. Tang, Singularity analysis of redundant parallel manipulators, *2004 IEEE International Conference on Systems*, (2004) 4214-4220.

[5] F. Q. Zhao, S. Guo, Z. C. Xu , et al., Design and analysis of high-performance machine tools based on redundant parallel mechanisms.

Journal of Central South University, 50 (01) (2019) 67-74.

[6] C. X. Yan, Q. Zhan and Z. Lu, Fault-tolerant method of parallel robot based on drive or structure redundancy[J]. *Journal of Beijing University of Aeronautics and Astronautics*, 36 (12) (2010) 1407-1411.

[7] X. M. Wang, G. H. Cui, H. J. Hou, et al., Research on Kinematic Statics and Singularity of Redundant Drive 2SPR-2RPU Parallel Mechanism[J], *Journal of Engineering Design*, 26 (5) (2019) 619-626.

[8] C. William, K. Erik, Metrics and Optimization of Internal Poses for Highly Redundant Truss-Like Serialized Parallel Manipulators. (2020) 1-6.

[9] H. Saafi, H. Lamine, Comparative Kinematic Analysis and Design Optimization of Redundant and Nonredundant Planar Parallel Manipulators Intended for Haptic Use, *Robotica*, 38(8) (2020) 1463-1477.

[10] N. Bahman, M. Farid and M. Mahzoon, Redundancy resolution and control of a novel spatial parallel mechanism with kinematic redundancy, *Mechanism and Machine Theory*, 133 (2018) 112-126.

[11] Y. Ping-Lang, et al., Optimization design for a compact redundant hybrid parallel kinematic machine, Robotics and Computer-Integrated Manufacturing, 58 (2019) 172-180.

[12] K. F. Wen, C. M. Gosselin, Forward Kinematic Analysis of Kinematically Redundant Hybrid Parallel Robots, *Journal of Mechanisms and Robotics*, 12(6) (2020) 1-11.

[13] K. F. Wen, C. Gosselin, Exploiting Redundancies for Workspace Enlargement and Joint Trajectory Optimisation of a Kinematically Redundant Hybrid Parallel Robot, *Journal of Mechanisms and Robotics*, (2021) 1-12.

[14] J. Landuré, C. Gosselin, Kinematic Analysis of a Novel Kinematically Redundant Spherical Parallel Manipulator, *Journal of Mechanisms and Robotics*, 10 (2) (2018) 1-10.

[15] M. Isaksson, C. Gosselin, K. Marlow, Singularity analysis of a class of kinematically redundant parallel Schönflies motion generators, *Mechanism and Machine Theory*, 112 (2017) 172-191.

[16] H. B. Qu, S. Guo, Y. Zhang, A novel relative degree-of-freedom criterion for a class of parallel manipulators with kinematic redundancy and its applications, *Journal of Mechanical Engineering Science*, 231 (22) (2016) 4227-4240.

[17]H. B. Qu, C. L. Zhang, S.Guo, Structural synthesis of a class of kinematically redundant parallel manipulators based on modified G–K criterion and RDOF criterion, *Mechanism and Machine Theory*,130 (2018) 47-70.

[18] Y. Q. Li, Y. Zhang, L. J. Zhang, A New Method for Type Synthesis of 2R1T and 2T1R 3-DOF Redundant Actuated Parallel Mechanisms with Closed Loop Units, *Chinese Journal of Mechanical Engineering*, 33 (1) (2020) 1-24.

[19] Q. M. Wang, J. Su, et al., Structural characteristics and kinematics analysis of a redundant 6-DOF parallel mechanism, *Chinese Journal of Mechanical Engineering*, 53(18) (2017) 121-130.

[20] P. Wang, Research on multi-objective optimization and decoupling control of 6-DOF redundant parallel mechanism, University of Electronic Science and Technology of China, (2018) 17-35.

[21]J. Wang, C. Gosselin, Kinematic Analysis and Design of Kinematically Redundant Parallel Mechanisms, *Journal of Mechanical Design*, Transactions of the ASME, 126 (1) (2004) 109-118.

[22] X. R. Li, J. Huang, X. H. Li, Kinematics and workspace analysis of a new 3-DOF redundant parallel mechanism, *Mechanical Transmission*, 43 (07) (2019) 130-135.

[23] L. T. Schreiber, C. Gosselin, Schnflies Motion Parallel Robot (SPARA): A Kinematically Redundant Parallel Robot With Unlimited Rotation Capabilities, *IEEE/ASME Transactions on Mechatronics*, 24 (5) (2019) 2273-2281.

[24] Y. F. Li, Q.Yang, X. Guo, Kinematics Research on a New Kind of Redundant Parallel Mechanism, *Machine Tool and Hydraulics*, 48 (09) (2020) 10-15.

[25] Y. M. Zhao, Z. L. Jin, Optimum design of wave energy conversion device based on 3-RPS/3-SPS parallel mechanism with redundant branches, *Chinese Journal of Mechanical Engineering*, 55 (23) (2019) 93-102.

[26] X. D. JIN, Y. F. FANG, D. ZHANG, Design and analysis of a class of redundant collaborative manipulators with 2D large rotational angles. *Frontiers of Mechanical Engineering*, 2020(1) 66-80.

[27] M. Z. Huang, J. T. Thebert, A study of workspace and singularity characteristics for design of 3-DOF planar parallel robots, *International Journal of Advanced Manufacturing Technology*, 51 (5-8) (2010) 789-797.

[28] H. B. Qu, L. Q. Hu, S. Guo, et al., Static Analysis of a Structural Redundant Planar Parallel Mechanism with Branched Closed Loops[J].*Journal of Central South University*, 51 (10) (2020) 2758-2771.

[29] N. Bahman, M. Mahzoon , and M. Farid, Singularity-Free Trajectory Planning of a 3- RP RR Planar Kinematically Redundant Parallel Mechanism for Minimum Actuated Effort, *Iranian Journal of Science & Technology Transactions of Mechanical Engineering*, (2018) 1-13.

[30] L. T. Schreiber, C. Gosselin, Kinematically redundant planar parallel mechanisms: Kinematics, workspace and trajectory planning, *Mechanism and Machine Theory*, 119 (2018) 91-105.

[31] N. Baron, A. Philippides, N. Rojas, A robust geometric method of singularity avoidance for kinematically redundant planar parallel robot manipulators, *Mechanism and Machine Theory*, 151 (2020) 1-14.

[32] M. Slavutin, A. Sheffer, Y. Reich, et al., A novel criterion for singularity analysis of parallel mechanisms, *Mechanism and Machine Theory*, 137 (2019) 459-475.

[33] X. L. Yang, H. T. Wu, B. Chen, et al., A dual quaternion approach to efficient determination of the maximal singularity-free joint space and workspace of six-DOF parallel robots, *Mechanism and Machine Theory*, 129 (2018) 279-292.

[34] Z. Zhang, Z. Shao, F. Peng, et al., Workspace Analysis and Optimal Design of a Translational Cable-Driven Parallel Robot With Passive Springs, *Journal of Mechanisms and Robotics*, 12 (5) (2020) 1-31.

[35] A. L. Orekhov, N. Simaan, Directional Stiffness Modulation of Parallel Robots With Kinematic Redundancy and Variable Stiffness Joints, *Journal of Mechanisms and Robotics*, 11 (5) (2019) 1-9.

[36] A. H. Dastjerdi, M. M. Sheikhi, and M. T. Masouleh, A complete analytical solution for the dimensional synthesis of 3-DOF delta parallel robot for a prescribed workspace, *Mechanism and Machine Theory*, 153 (2020):103991.

[37] A. Peidró, Ó. Reinoso, A. G. José, et al., A Simulation Tool to Study the Kinematics and Control of 2RPR-PR Parallel Robots, *Ifac*

Papersonline, 49 (6) (2016) 268-273.